Imaging by target-oriented wave-equation inversion: 3-D field data results

Alejandro A. Valenciano, Biondo L. Biondi, and Robert G. Clapp Stanford University*

SUMMARY

Wave-equation inversion is a powerful technique able to build clean images with balanced amplitudes in complex subsurface areas relative to migration alone. This paper illustrates how to perform wave-equation inversion in image space without making any velocity model or acquisition geometry approximations. The method explicitly computes the least-squares Hessian matrix, defined from the modeling/migration operators, and uses an iterative solver to find the solution of the resulting system of equations. This technique can handle 3-D data in a target-oriented fashion. The inversion in the presence of a complex overburden leads to an ill-conditioned system of equations that needs to be regularized to obtain a stable numerical solution. Regularization can be implemented in the poststack image-domain (zero subsurface offset), where the options for a regularization operator are limited to a customary damping, or in the prestack image-domain (subsurface offset), where a physically-inspired regularization operator (differential semblance) can be applied. Though the prestack image-domain inversion is more expensive than the poststack image-domain inversion, it can improve the reflectors continuity into the shadow zones with an enhanced signal-to-noise ratio. We demonstrate the utility of both these methods by improving the subsalt-sediment images of a 3-D Gulf of Mexico field data set.

INTRODUCTION

Seismic imaging (modeling/migration) operators are non-unitary (Claerbout, 1992, 1985, 2001), meaning that if $\mathbf{L}$ is a modeling operator, and $\mathbf{L}'$ is its adjoint (migration), their product $\mathbf{L}'\mathbf{L} \neq \mathbf{I}$, where $\mathbf{I}$ is the identity matrix. As a result, images of the subsurface are blurred when produced by a migration operator. Even for a simple subsurface, the bandlimited characteristic of the seismic data in the time and space domain would prevent $\mathbf{L}$ and $\mathbf{L}'$ from being unitary (Claerbout, 1985; Chavent and Plessix, 1999; Plessix and Mulder, 2004). Moreover, where the subsurface is complex, and the seismic acquisition geometry is limited and irregular, the non-unitary characteristic of the imaging operators causes migration to produce images with artifacts and biased amplitudes.

One way to improve on the use of an adjoint operator such as that for migration is to use inversion (Tarantola, 1987). The "relative reflectivity" can be inverted from the seismic data to obtain images that better represent the subsurface properties and geometry than do those from migration (Nemeth et al., 1999; Prucha and Biondi, 2002; Kuhl and Sacchi, 2003; Clapp, 2005). The assumption behind the reflectivity inversion (as for migration) is that the long-wavelength model (migration velocity) is known.

Solution of the Ill-posed inversion problem

Solving linear systems generally is not difficult, but the high dimensionality and the ill-posedness of the seismic-imaging inverse problem in complex areas, makes its solution challenging. There are two main physical reasons for this. The first is the limited and irregular acquisition geometry of the seismic experiment (Nemeth et al., 1999; Duquet and Marfurt, 1999; Ronen and Liner, 2000). The second is the complexity of the overburden (Rickett, 2003; Guitton, 2004; Clapp, 2005). These two effects combined produce incomplete and irregular illumination of the subsurface. In the worst cases "shadow zones" can be created.

Two main lines of attack to solve the inverse problem have been discussed in the literature, both based on least-squares. The first is to approximate the inverse of the least-squares Hessian ($\mathbf{L}'\mathbf{L}$) to reduce the computational cost. Hu et al. (2001) introduced a horizontally invariant non-diagonal Hessian for $v(z)$ media; Rickett (2003) proposed to compute a diagonal Hessian from reference images; Plessix and Mulder (2004) proposed to compute a diagonal Hessian using analytical approximations for the contribution of the receiver-side Green's functions; and Guitton (2004) used a bank of non-stationary matching filters to approximate a non-diagonal inverse of the Hessian. The second type of approach is computationally more challenging but can deliver a better performance. It finds the least-squares solution by means of an iterative solver. Nemeth et al. (1999) first proposed this approach using Kirchhoff operators; more recently, Prucha and Biondi (2002), Kuhl and Sacchi (2003), and Clapp (2005) proposed to use wave-equation operators that seem more suitable for complex areas.

Since accurate imaging of reflectors is most important at the reservoir level, we propose to explicitly compute an approximation of the Hessian in a target-oriented fashion (Valenciano et al., 2006). Computing the Hessian in a region of the model space allows reduction of the Hessian matrix size by a large factor, thereby, allowing reduction in the number of approximations used in its computation. After we compute a non-diagonal Hessian matrix, we use an iterative algorithm to obtain the inverse image.

The discretization of the ill-posed least-squares inversion produces an ill-conditioned system of equations (Hanke, 1995). The conventional approach to that problem is to stabilize it by using some form of regularization (Tikhonov and Arsenin, 1977). Regularization also has its statistical interpretation, that of adding prior information on the model covariance, in this case on the properties of the reflectivity. From the results reported by Prucha and Biondi (2002), Kuhl and Sacchi (2003), and Clapp (2005), a regularization in the prestack image domain (reflection-angle) can help to stabilize the inversion.

LINEAR LEAST-SQUARES INVERSION

Linear least-squares inversion provides a theoretical approach to compensating for experimental deficiencies (e.g., limited

acquisition geometry), and complexities of the overburden, while maintaining consistency with the acquired data. For seismic imaging, it can be summarized as follows. Given a linear modeling operator $\mathbf{L}$, compute synthetic data $\mathbf{d}$ using, $\mathbf{d} = \mathbf{L}\mathbf{m}$, where $\mathbf{m}$ is a reflectivity model.

The quadratic cost function,

$$S(\mathbf{m}) = \|\mathbf{d} - \mathbf{d}_{obs}\|^2 = \|\mathbf{L}\mathbf{m} - \mathbf{d}_{obs}\|^2, \quad (1)$$

is formed, where $\mathbf{d}_{obs}$ denotes the recorded data.

Up to this point, no prior information about the covariance of the model (model regularization) has been included in the definition of the cost function. We will ignore the need of regularization here, but in a later subsection, we will show how to add regularization to solve the otherwise ill-posed inversion problem.

The reflectivity model $\hat{\mathbf{m}}$ that minimizes $S(\mathbf{m})$ is given by

$$\hat{\mathbf{m}} = (\mathbf{L}'\mathbf{L})^{-1}\mathbf{L}'\mathbf{d}_{obs} = \mathbf{H}^{-1}\mathbf{m}_{mig}, \quad (2)$$

where $\mathbf{L}'$ (the migration operator) is the adjoint of the linear modeling operator $\mathbf{L}$, $\mathbf{m}_{mig}$ is the migration image, $\mathbf{m}_{mig} = \mathbf{L}'\mathbf{d}_{obs}$, and $\mathbf{H} = \mathbf{L}'\mathbf{L}$ is the Hessian of $S(\mathbf{m})$.

Since the model space can be large, computing the inverse of the Hessian matrix is a big challenge for most geophysical imaging problems. For this reason, it is often more feasible to compute the inverse image as the solution of the linear system of equations

$$\mathbf{H}\hat{\mathbf{m}} = \mathbf{m}_{mig}, \quad (3)$$

by using an iterative inversion algorithm. Again the conjugate-gradient method can be used; however, this time only one matrix-vector multiplication of the Hessian matrix with the model vector is necessary per iteration. Still, explicit computation of the Hessian for the entire model space is too expensive in practice. Valenciano (2008) discuss how exploiting the structure of the Hessian matrix and the localization in the model space makes this problem tractable.

Regularization

Two different regularization schemes for wave-equation inversion have been discussed in the literature. First is the use of a weighted identity operator, which is customary in many scientific applications (damping). The second is a *geophysical regularization*, which imposes smooth variation of the image in the offset ray-parameter dimension (which is equivalent to the reflection-angle dimension) (Prucha and Biondi, 2002; Kuhl and Sacchi, 2003; Clapp, 2005). A third regularization can be designed in analogy to the work of Stolk and Symes (2002), and Shen et al. (2003), in nonlinear wave-equation inversion for velocity estimation. It is a differential semblance operator to penalize the energy in the image not focused at zero subsurface offset. In this paper we choose to compare only the first and the third options for regularization.

The prestack image-domain version of equation 3 with a general regularization can be stated as

$$\left(\mathbf{H}(\mathbf{x},\mathbf{h};\mathbf{x}',\mathbf{h}') + \varepsilon\mathbf{R}\right)\hat{\mathbf{m}}(\mathbf{x},\mathbf{h}) - \mathbf{m}_{mig}(\mathbf{x},\mathbf{h}) = \mathbf{r} \approx 0, \quad (4)$$

where $\mathbf{H}(\mathbf{x},\mathbf{h};\mathbf{x}',\mathbf{h}')$ is the subsurface-offset Hessian, $\mathbf{R}$ is a linear regularization operator, $\mathbf{x} = (x,y,z)$ is a point in the image, $\mathbf{h} = (h_x,h_y,h_z)$ is the half subsurface offset, $\mathbf{r}$ is the residuals vector, and ε is a scalar parameter that governs the strength of the regularization.

The first option for the regularization operator is a customary damping, given by $\mathbf{R} = \mathbf{I}$, where $\mathbf{I}$ is the identity operator (Valenciano et al., 2006). However all the extra cost involved in expanding the dimensionality of equation 3 is justified when moving beyond damping. The third regularization option is a differential semblance operator, defined as $\mathbf{R} = \mathbf{P}_\mathbf{h}^2$, where $\mathbf{P}_\mathbf{h} = |\mathbf{h}|$ is the differential semblance operator (Shen et al., 2003). It penalizes the energy in the image not focused at zero subsurface offset.

THE 3-D GULF OF MEXICO DATA

The 3-D velocity model corresponding to the subset of the data can be seen in Figure 1. The salt body on the right side causes significant shadow zones that can mask potential hydrocarbon reservoirs. The velocity model is believed to be accurate, which is important given the linearity of the operators assumption with respect to the background velocity used to derive the Hessian. We choose a target zone (indicated with the "target" box in Figure 1) to test how the inversion performs in imaging the subsalt sediments. The dimensions of the target volume are 3630 ft in depth, 12303 ft in the x-dimension, and 4101 ft in the y-dimension.

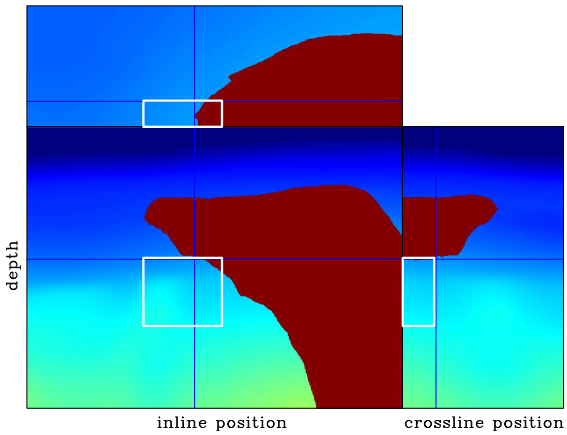

Figure 1: Velocity model for the 3-D Gulf of Mexico data; target zone indicated with the "target" box.

The data that contributed to the migration were small subset of the data provided by BP and ExxonMobil, it did not have crossline offset because they were regularized by using an azimuth moveout (AMO) algorithm (Biondi et al., 1998). The frequency content ranged between 5 Hz and 35 Hz, with 20 Hz being the dominant frequency.

The 3-D Hessian matrix

Figure 2 shows the diagonal of the Hessian matrix for the 3-D target-zone. Note the complexity of the focusing and defocus-

ing of the seismic energy produced by the rugosity of the bottom of the salt. Figure 3 shows the off-diagonal terms (point spread function) off the 3D Hessian matrix at 72 point scatterers positions. The spread of the energy caused by the 3-D geometry of the salt body is clearly non-stationary. Note that the resolution in the crossline direction is poorer than that in the inline direction, as a result of the crossline limited data coverage.

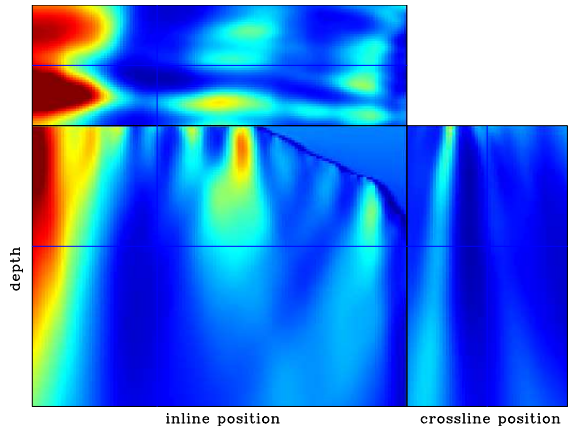

Figure 2: Diagonal of the Hessian in the target area. Cool colors represent areas with low values, and warm colors represent areas with high values.

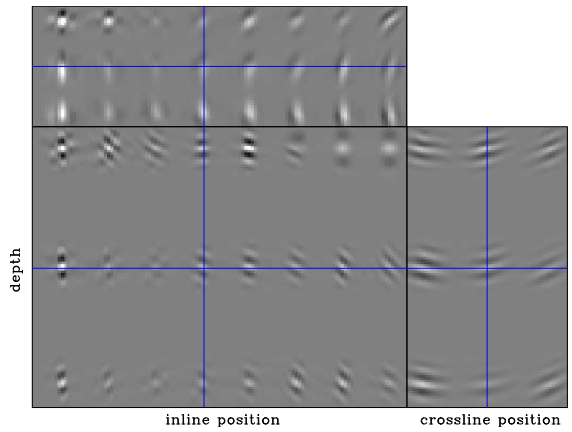

Figure 3: Convolution of the 72-point-scatterer model with the 3-D Hessian matrix. Notice the non-stationarity of the PSF.

We used just 11 frequencies to compute the Green's functions for calculating the 3-D Hessian. The frequency band was chosen between 10 and 31 Hz, with a sampling interval of 2 Hz. The frequency sampling was fine enough to avoid contamination from wrap-around artifacts in the off-diagonal terms of the Hessian matrix (Valenciano, 2008).

Inversion in the poststack image domain

Here we solve the linear system in equation 4 by using the method of conjugate gradients. The right-hand-side vector is the migrated image at zero subsurface offset (Figures 4a). The Hessian matrix contains only 2-D PSFs ($na_x = 15, na_y = 1, na_z = 30$), thus implying there is no correlation between neighboring points in the crossline direction. This assumption decreases the size of the Hessian matrix by at least two orders of magnitude. The inversion result is shown in Figure 4b; its benefits are evident compared to the migrations in Figures 4a. The choice of the regularization parameter $\varepsilon = 0.1$ decreases the residuals and stabilizes the inversion.

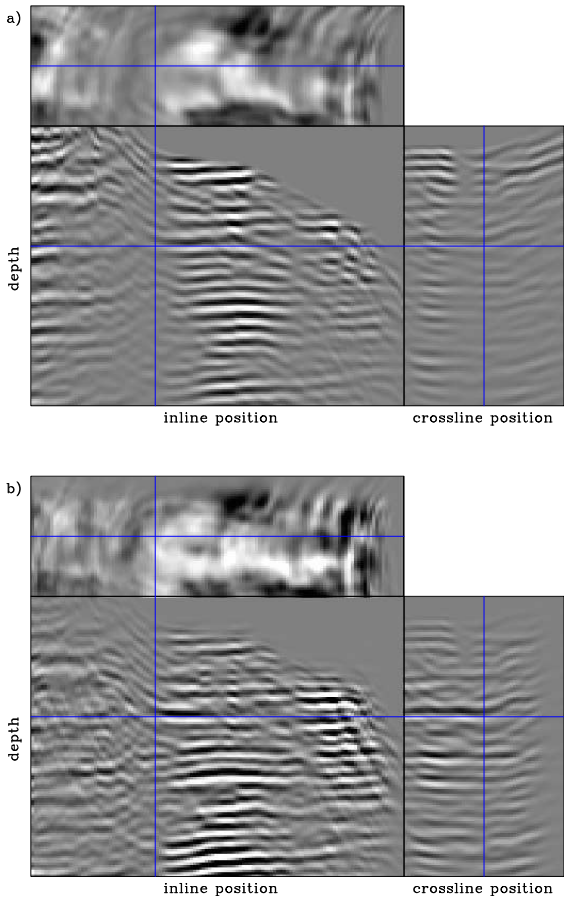

Figure 4: Zero subsurface-offset image of the 3-D Gulf of Mexico data: a) 3-D shot profile migration, and b) 3-D inversion in the poststack-image domain with 2-D PSFs. Notice the improved balance and resolution in the inversion image.

Overall, the inversion shows more balanced amplitudes than does the migration, allowing continuation of the reflector inside the shadow zones. It also reduces some of the migration smiles, specially in the inline direction. The reflectors gain vertical and horizontal resolution, making them more interpretable. Improving the coherence of the events in the inline direction also improves the coherence in the crossline direction. However, no resolution is gained in this dimension, since the spread in the crossline is not included in the inversion.

Inversion with regularization in the prestack image domain

When imaging under complex salt structures, it is useful to compute image gathers in the subsurface offset or the reflection and azimuth angle. Depending on the geometry of the salt the angle gathers can have illumination gaps; a good regular-

ization of the wave-equation inversion can be to extend the image from well-illuminated to poorly illuminated angles. In this section, we apply it to the inversion of the 3-D Gulf of Mexico data. We limit the subsurface offset to the inline direction, and the angle to the reflection angle due to limited computational resources. The methodology presented here can be generalized to crossline subsurface offset and azimuth angle.

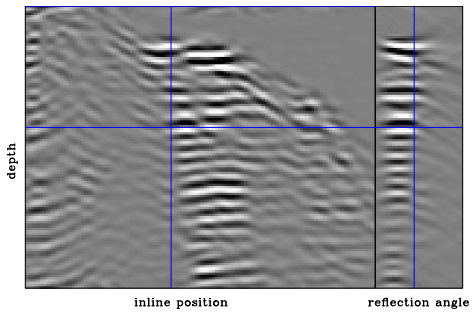

Figure 5: Migrated image in the reflection-angle domain after offset-to-angle transformation.

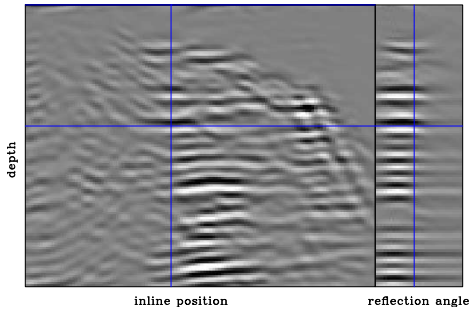

Figure 6: Inverted image in the subsurface-offset domain, after an offset-to-angle transformation.

The expansion in the dimensionality of the model space increases the cost of the inversion by a order of magnitude. In the next numerical experiments the Hessian matrix contains only the 2-D PSF ($na_x = 15, na_y = 1, na_z = 30$), and the model space is 4-D, with the extra dimension being the subsurface offset. We show the results after an offset-to-angle transformation, since the reflection angle has more physical meaning than the subsurface offset.

Figure 5 shows an reflection-angle gather (side panel) corresponding to a crossline position in the 4-D migration cube. Notice the narrow range and the irregularity of the angle illumination. Figure 6 shows the inverted image obtained after an offset-to-angle transformation. We solved the linear system in equation 4 in the subsurface-offset domain, with differential semblance as the regularization operator and $\varepsilon = 0.5$. Comparing this result with the migration, we see that the inversion plus regularization equalizes the amplitudes in the angle gathers, filling the illumination gaps in the shadow zone. Also we see an increase in vertical and lateral resolution.

The last two figures, Figures 7a and 7b, show the comparison of the angle-stack of the migration with the angle-stack of the inversion. Whereas they couldn't be done in the migration results, some of the reflectors can be traced almost entirely through the shadow zones in the inversion results.

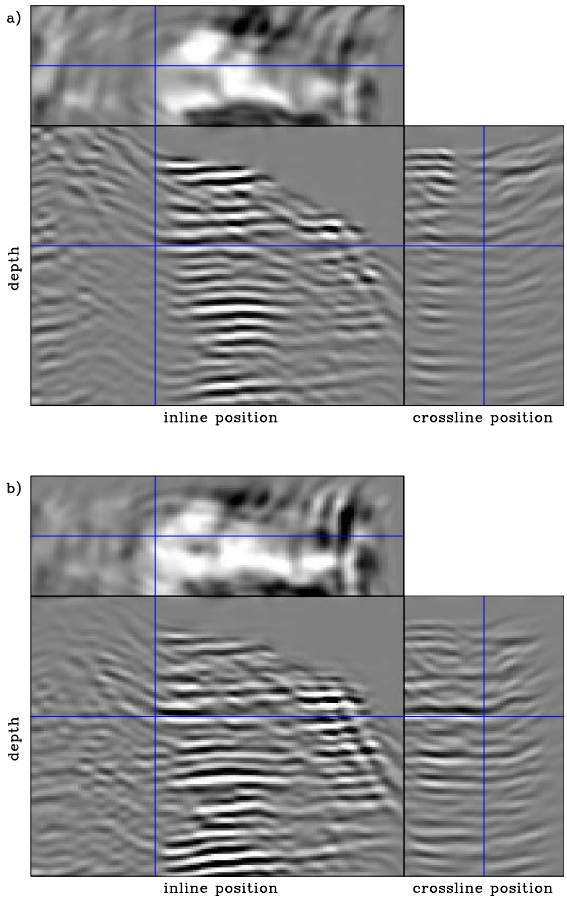

Figure 7: Comparison of the angle-stack of a) the migration, with b) the inversion in the subsurface-offset domain, after an offset-to-angle transformation with regularization parameter $\varepsilon = 0.5$.

CONCLUSIONS

Wave-equation inversion can be done in image space without making any velocity model or acquisition geometry approximations. We conclude that the regularization with the differential semblance in the subsurface-offset domain, although it is more expensive, can improve the continuity of the reflectors into the shadow zones with a higher signal-to-noise ratio than can regularization in the poststack image-domain (zero subsurface offset). This does not means that the regularization in the poststack image-domain cannot be an economical alternative for 3-D data.

ACKNOWLEDGMENTS

Thanks to BP and ExxonMobil for the field data.

EDITED REFERENCES

Note: This reference list is a copy-edited version of the reference list submitted by the author. Reference lists for the 2008 SEG Technical Program Expanded Abstracts have been copy edited so that references provided with the online metadata for each paper will achieve a high degree of linking to cited sources that appear on the Web.

REFERENCES

Biondi B., S. Fomel, and N. Chemingui, 1998, Azimuth moveout for 3D prestack imaging: Geophysics, **63**, 574–588.

Chavent, G., and R. E. Plessix, 1999, An optimal true-amplitude least-squares prestack depth-migration operator: Geophysics, **64**, 508–515.

Claerbout, J. F., 1985, Imaging the Earth's interior: Stanford Exploration Project.

———1992, Earth soundings analysis, processing versus inversion: Blackwell Scientific Publications.

———2001, Basic Earth imaging: Stanford Exploration Project.

Clapp M. L., 2005, Imaging under salt: Illumination compensation by regularized inversion: Ph.D. thesis, Stanford University.

Duquet, B., and K. J. Marfurt, 1999, Filtering coherent noise during prestack depth migration: Geophysics, **64**, 1054–1066.

Guitton, A., 2004, Amplitude and kinematic corrections of migrated images for nonunitary imaging operators: Geophysics, **69**, 1017–1024.

Hanke, M., 1995, Conjugate gradient type methods for ill-posed problems: Longman Scientific and Technical.

Hu, J., and G. T. Schuster, and P. A. Valasek, 2001, Poststack migration deconvolution: Geophysics: **66**, 939–952.

Kuhl, H., and M. D. Sacchi, 2003, Least-squares wave-equation migration for AVP/AVA inversion: Geophysics, **68**, 262–273.

Nemeth, T., C. Wu, and G. T. Schuster, 1999, Least-squares migration of incomplete reflection data: Geophysics, **64**, 208–221.

Plessix, R. E., and W. A. Mulder, 2004, Frequency-domain finite-difference amplitude-preserving migration: Geophysical Journal International, **157**, 975–987.

Prucha, M., and B. L. Biondi, 2002, Subsalt event regularization with steering filters: 72nd Annual International Meeting, SEG, Expanded Abstracts, 922–925.

Rickett, J., 2003, Illumination-based normalization for wave-equation depth migration: Geophysics, **68**, 1371–1379.

Ronen, S., and C. L. Liner, 2000, Least-squares DMO and migration: Geophysics, **65**, 1364–1371.

Shen, P., W. Symes, and C. Stolk, 2003, Differential semblance velocity analysis by wave-equation migration: 73rd Annual International Meeting, SEG, Expanded Abstracts, 2132–2135.

Stolk, C., and W. Symes, 2002, Theory of differential semblance velocity analysis by wave equation migration: TRIP Annual Report.

Tarantola, A., 1987, Inverse problem theory: Methods for data fitting and model parameter estimation: Elsevier.

Tikhonov, A. N., and V. Y. Arsenin, 1977, Solution of ill-posed problems: John Wiley and Sons.

Valenciano A. A., 2008, Imaging by wave-equation inversion: Ph.D. thesis, Stanford University.

Valenciano, A. A., B. L. Biondi, and A. Guitton, 2006, Target-oriented wave-equation inversion: Geophysics, **71**, A35–A38.